Bifurcation Analysis of the Fractional Duffing System Based on the Improved Short Memory Principle Method

Ruiqun Ma
NUAA: Nanjing University of Aeronautics and Astronautics
Bo Zhang
NUAA College of Aerospace Engineering: Nanjing University of Aeronautics and Astronautics College of Aerospace Engineering
Haiwei Yun
NUAA College of Aerospace Engineering: Nanjing University of Aeronautics and Astronautics College of Aerospace Engineering
Jinglong Han (hjlae@nuaa.edu.cn)
NUAA College of Aerospace Engineering: Nanjing University of Aeronautics and Astronautics College of Aerospace Engineering

Research Article

Keywords: Fractional calculus, Bifurcation, Chaos, Short memory principle

Posted Date: June 8th, 2021

DOI: https://doi.org/10.21203/rs.3.rs-580152/v1

Bifurcation analysis of the fractional Duffing system based on the improved short memory principle method

Ruiqun Ma, Bo Zhang, Haiwei Yun, Jinglong Han*
Ruiqun Ma
State Key Laboratory of Mechanics and Control of Mechanical Structures
Nanjing University of Aeronautics and Astronautics, Nanjing 210016, China
Bo Zhang
State Key Laboratory of Mechanics and Control of Mechanical Structures
Nanjing University of Aeronautics and Astronautics, Nanjing 210016, China
Haiwei Yun
State Key Laboratory of Mechanics and Control of Mechanical Structures
Nanjing University of Aeronautics and Astronautics, Nanjing 210016, China
Jinglong Han(✉)
State Key Laboratory of Mechanics and Control of Mechanical Structures
Nanjing University of Aeronautics and Astronautics, Nanjing 210016, China
e-mail: hjlae@nuaa.edu.cn

Abstract In this study, the improved short memory principle method is introduced to the analysis of the dynamic characteristics of the fractional Duffing system, and the basis for the improvement of the short memory principle method is provided. The influence of frequency change on the dynamic performance of the fractional Duffing system is studied using nonlinear dynamic analysis methods, such as phase portrait, Poincare map and bifurcation diagram. Moreover, the dynamic behaviour of the fractional Duffing system when the fractional order and excitation amplitude change is investigated. The analysis shows that when the excitation frequency changes from 0.43 to 1.22, the bifurcation diagram contains four periodic and three chaotic motion regions. Periodic motion windows are found in the three chaotic motion regions. Results confirm that the frequency and amplitude of the external excitation and the fractional order of damping have a greater impact on system dynamics. Thus, attention should be paid to the design and analysis of system dynamics.

Keywords Fractional calculus, Bifurcation, Chaos, Short memory principle

1. Introduction

Fractional calculus was proposed almost at the same time as integer calculus. Its development was relatively slow for nearly 300 years due to the lack of a clear physical meaning of fractional calculus, and it was mainly studied in the field of pure mathematics. In 1974, Oldham and Spanier [1] co-authored the first monograph on fractional calculus titled 'Applied Fractional Calculus', which paved the way toward the application of fractional calculus. In the 1970s, Mandelbrot [2] pointed out that many fractional dimensions exist in nature. Since then, the theory of fractional calculus has developed rapidly, and numerous applications of fractional calculus have emerged [3]-[9]. The application of fractional calculus in mechanical engineering has gradually increased in recent years mainly because many physical objects have fractional characteristics, such as viscoelasticity, damping, mechanical friction and impact [10]-[12].

Many popular fractional systems, such as the Rossler system, the Lorenz system, Chua's circuit and the Duffing system, have been used for research. The Duffing system has been applied in many fields, including fluid-induced vibration, large-amplitude oscillation of centrifugal speed control systems and mathematical modelling [20]-[22]. The Duffing system that considers fractional differential damping is equivalent to introducing polymer damping into the classic Duffing system. Compared with the traditional integer-order damping model, the fractional-order damping model can more accurately describe the dynamic behaviour of a system [23]-[25]. In Reference [26], the nonlinear dynamic behaviour of the fractional-order Duffing system was studied using the Adams–Bashforth–Moulton predictor–corrector method. The Adomian decomposition method was utilised to find the numerical solution to the combined fractional differential equation of the Duffing equation and the Van der Pol equation in Reference [27]. The Melnikov method transforms a fractional-order system into an equivalent integer-order system, which can effectively detect chaos in the fractional-order Duffing system [28].

In this study, the improved short memory principle method is used to study the dynamic characteristics of the fractional Duffing system. Firstly, the Grünwald–Letnikov definition of fractional calculus is adopted. Secondly, the classical short memory principle is improved, and the numerical solution of the system is obtained. Lastly, the influence of excitation frequency on the dynamic performance of the fractional Duffing system is studied using nonlinear dynamic analysis methods, such as phase portrait, Poincare map and bifurcation diagram. Moreover, the dynamic behaviour of the fractional Duffing system when the external excitation amplitude and fractional order change is investigated.

2. Fractional Duffing System

2.1 Fractional Differential Definition

The three most frequently used definitions for fractional derivatives are Grünwald–Letnikov, Riemman–Liouville and Caputo definitions. The Grünwald–Letnikov definition is used in this work, as it is expressed as

$$ {}_{t_0}^{GL}D_t^{\alpha}x(t) = \lim_{h\to 0}\frac{1}{h^{\alpha}}\sum_{j=0}^{[(t-t_0)/h]}(-1)^j\binom{\alpha}{j}x(t-jh) \tag{1} $$

where α is the fractional order, h is the time step and [·] means rounding. If time step h is small enough, the above-mentioned formula can be written as

$$ {}_{t_0}^{GL}D_t^{\alpha}x(t) \approx \frac{1}{h^{\alpha}}\sum_{j=0}^{[(t-t_0)/h]} w_j\, x(t-jh) \tag{2} $$

where w_j is the coefficient of binomial $(1-z)^{\alpha}$.

$$ w_j = (-1)^j\binom{\alpha}{j} \tag{3} $$

Equation (3) is changed to the recursive form

$$ w_j = \left(1-\frac{\alpha+1}{j}\right)w_{j-1} \tag{4} $$

Its first item $w_0 = 1$.

2.2 Improved Short Memory Principle Method

The classical short memory principle truncates the memory time. In Equation (2), the upper limit of summation becomes $[L/h]$, where L is the fixed memory time length, and the part exceeding L is discarded. The discarded part often brings errors

that cannot be ignored. In particular, when fractional order α approaches zero, the binomial coefficient changes slowly.

The improved short memory principle method changes the truncation of the memory time in the classic short memory principle to the number of terms of the binomial coefficient. Then, the finite binomial coefficient is repeatedly applied to gradually enlarging time steps for error reduction. The expression of a time step being enlarged for the first time is

$$D_t^\alpha x(t) = \frac{1}{h^\alpha}\sum_{j=0}^{N} w_j\, x(t-jh) + \frac{1}{(mh)^\alpha}\sum_{j=\left[\frac{N}{m}\right]+1}^{[t/(mh)]} w_j\, x(t-jmh) \tag{5}$$

The definition of Grünwald–Letnikov is used in this study, and the formulas are no longer marked. In Equation (5), N is the number of binomial truncated terms and m is the magnification of the step length. Similarly, the expression of the second enlargement of step size is

$$\begin{aligned} D_t^\alpha x(t) = {} & \frac{1}{h^\alpha}\sum_{j=0}^{N} w_j\, x(t-jh) + \frac{1}{(mh)^\alpha}\sum_{j=\left[\frac{N}{m}\right]+1}^{N} w_j\, x(t-jmh) \\ & + \frac{1}{(m^2h)^\alpha}\sum_{j=\left[\frac{N}{m}\right]+1}^{[t/(m^2h)]} w_j\, x(t-jm^2h) \end{aligned} \tag{6}$$

In the same manner, we can derive other expressions of step size.

2.3 Basis for Step Enlargement

Step enlargement is based on the initial time step. After the step size is enlarged, although the interval for taking the function value increases, the binomial coefficient of the function value also increases, and the magnification is almost the same as the step size magnification. For example, Equation (5) can be rewritten as

$$D_t^\alpha x(t) = \frac{1}{h^\alpha}\left(\sum_{j=0}^{N} w_j\, x(t-jh) + \sum_{j=\left[\frac{N}{m}\right]+1}^{[t/(mh)]} \frac{w_j}{m^\alpha} x(t-jmh)\right) \tag{7}$$

The second term at the right end of the formula above is the result of the step size being enlarged for the first time. The binomial coefficient before the function value

$x(t-jmh)$ is w_j/m^{α}. If the step size is not enlarged, the binomial coefficient in front of the function value should be w_{jm}. Table 1 shows the ratio of the corresponding binomial coefficients when $N=100$, $\alpha=0.5$ and m are 5, 10 and 20, respectively. A is the ratio of binomial coefficient w_j/m^{α} after the first step is enlarged to binomial coefficient w_{jm} without enlargement. B is the ratio of binomial coefficient $w_j/m^{2\alpha}$ after the second step is enlarged to binomial coefficient w_{jm^2} without enlargement. The ratio is almost equal to step magnification m and m^2, and the ratio increases with the increase in step magnification. With the increase in magnification, the first binomial coefficient increases; in particular, when n=20, it is larger than the number of initial steps in the enlarged step. A large magnification causes a large error. In addition, whether the adopted function value is representative in the interval, that is, whether the adopted function value is close to the average value of the function value in the interval, is also a question to be considered. The error in the long-term calculation is limited because expanding the step size to derive the function value is a dynamic ergodic process. In summary, we should try to intercept as many binomial coefficients as possible if the calculation conditions permit and select a small step size magnification to obtain a highly accurate numerical solution.

Table 1 Partial results of $\frac{w_j/m^{\alpha}}{w_{jm}}$ and $\frac{w_j/m^{2\alpha}}{w_{jm^2}}$ when α = 0.5

$m=5$			$m=10$			$m=20$		
j	$\frac{w_j/m^{\alpha}}{w_{jm}}$	$\frac{w_j/m^{2\alpha}}{w_{jm^2}}$	j	$\frac{w_j/m^{\alpha}}{w_{jm}}$	$\frac{w_j/m^{2\alpha}}{w_{jm^2}}$	j	$\frac{w_j/m^{\alpha}}{w_{jm}}$	$\frac{w_j/m^{2\alpha}}{w_{jm^2}}$
						6	21.302	427.31
			11	10.3225	103.543	11	20.6804	414.279
21	5.07335	25.4396	21	10.1649	101.813	21	20.348	407.306
31	5.04926	25.2953	31	10.1108	101.218	31	20.2338	404.909
41	5.03708	25.2224	41	10.0834	100.917	41	20.176	403.696
51	5.02973	25.1783	51	10.0669	100.735	51	20.1412	402.964
61	5.02481	25.1488	61	10.0558	100.614	61	20.1178	402.474
71	5.02129	25.1277	71	10.0479	100.527	71	20.1011	402.123
81	5.01865	25.1118	81	10.0419	100.461	81	20.0885	401.859
91	5.01658	25.0995	91	10.0373	100.41	91	20.0788	401.654
100	5.01508	25.0905	100	10.0339	100.373	100	20.0716	401.504

2.4 Fractional Duffing System

The form of the classic integer-order Duffing system is

$$mD^2(t) + cDx(t) + kx(t) + ax^3(t) = f\ \sin(\omega t) \quad (8)$$

where D is the first-order differential operator, D^2 is the second-order differential operator, m is the mass, c is the damping coefficient, k is the linear stiffness coefficient, a is the nonlinear stiffness coefficient and f and ω are the amplitude and frequency of external excitation, respectively. If the damping term is changed to the fractional order, it becomes a fractional-order Duffing system.

$$mD^2x(t) + cD^\alpha x(t) + kx(t) + ax^3(t) = f\ \sin(\omega t) \quad (9)$$

where α is the fractional order of the damping of the fractional Duffing system. In this study, we use the improved short memory principle to solve the fractional Duffing equation.

3. Nonlinear Dynamic Analysis of the Fractional Duffing System

In this section, several of the fixed parameters in Equation (9) are taken as $m = 1$, $c = 0.9$, $k = -1$ and $a = 1$. The initial conditions are $x(0) = 0$ and $\dot{x}(0) = 0$.

3.1 Excitation Frequency ω is the Variable Parameter

Fractional order $\alpha = 1.2$ and excitation amplitude $f = 0.6$ are adopted to analyse the influence of excitation frequency on the system. The calculation parameters are as follows: the basic step size is $h = 0.001$, the number of truncated items is $Nt = 10{,}000$ and the step length magnification is $m = 5$. Excitation frequency ω is changed from 0.43 to 1.23 in the experiment to analyse the influence of excitation frequency on the fractional Duffing system, and the change step is 0.001. A total of 250 cycles are calculated for each frequency point, and the first 150 cycles are discarded. The bifurcation diagram of the system obtained with ω as the control parameter is shown in Fig. 1.

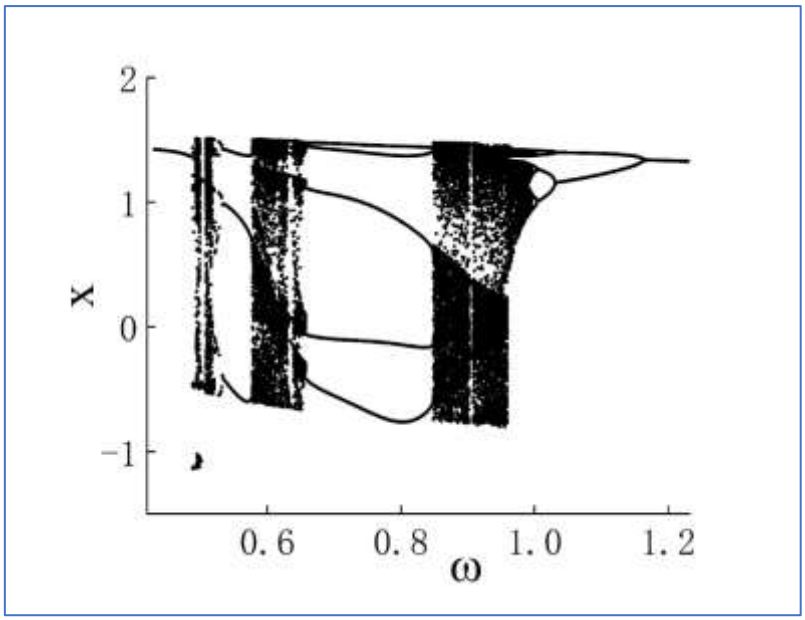

Fig.1 Bifurcation diagram of the fractional-order Duffing system with $\alpha = 1.2,\ 0.43 < \omega \leq 1.23$

The figure indicates that excitation frequency ω has a relatively large impact on the dynamic behavior of the system. Three chaotic and four periodic motion regions exist during the change of ω from 0.43 to 1.22. The performance of the system in response to stable period-1 motion occurs at $0.43 < \omega \leq 0.487$. The phase portrait and Poincaré map when $\omega = 0.45$ are shown in Figs. 2(a1) and 2(a2), respectively. The phase portrait is a universal limit cycle; correspondingly, the Poincaré map exhibits an isolated point. Notably, $0.488 < \omega \leq 0.518$ is the first chaotic motion region of the system. The phase portrait and Poincaré map when $\omega = 0.509$ are shown in Figs. 2(b1) and 2(b2), respectively. On the Poincaré map, many discrete points are concentrated in two areas. With the increase in excitation frequency ω, the system enters the period-3 motion region, that is, at $0.519 \leq \omega \leq 0.577$. The phase portrait and Poincaré map when $\omega = 0.55$ are shown in Figs. 2(c1) and 2(c2), respectively. The Poincaré map appears as three isolated points, and $0.578 \leq \omega \leq 0.657$ is the second chaotic region of the system. The phase portrait when $\omega = 0.6$ is shown as Fig. 2(d1), and scattered points can be seen on the corresponding Poincaré map in Fig. 2(d2). When $\omega \geq 0.658$, the system enters a stable period-5 motion region, and its interval is $0.658 \leq \omega \leq 0.848$. The phase portrait and Poincaré map when $\omega = 0.8$ are shown in Figs. 2(e1) and 2(e2), respectively. The Poincaré map has five scattered points, and

$0.849 \leq \omega \leq 0.995$ is the third chaotic motion region. Fig. 2(f1) shows the phase portrait when $\omega = 0.88$, and the corresponding Poincaré map is given in Fig. 2(f2). As ω further increases, the system enters periodic motion from chaotic motion. Fig. 1 indicates that when $\omega \geq 1.17$, the system moves stably in period 1. A period-doubling bifurcation transition region exists between the periodic motion region and the third chaotic motion region. The phase portrait and Poincaré map of the transition region when $\omega = 1.02$ are shown in Figs. 2(g1) and 2(g2), respectively.

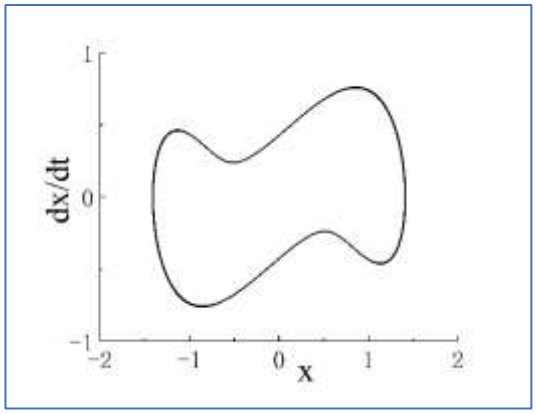

(a1)

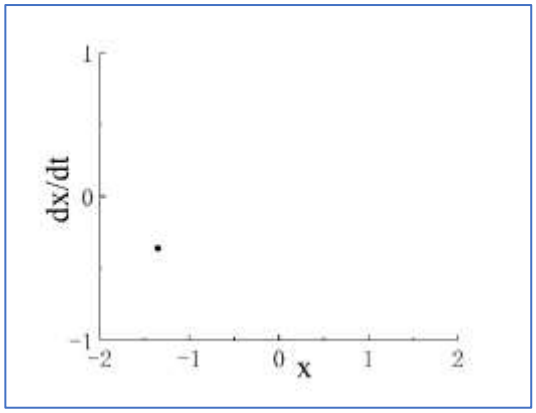

(a2)

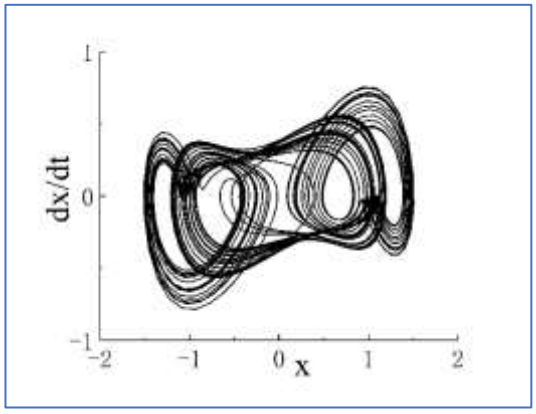

(b1)

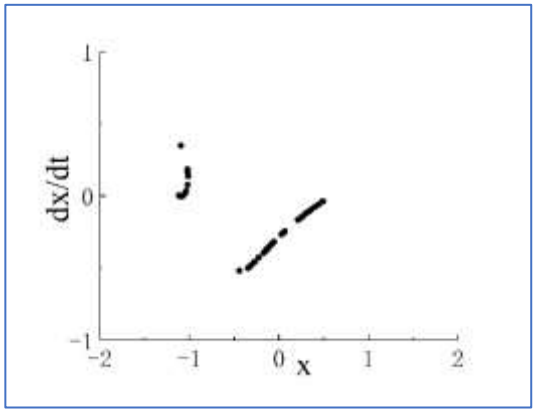

(b2)

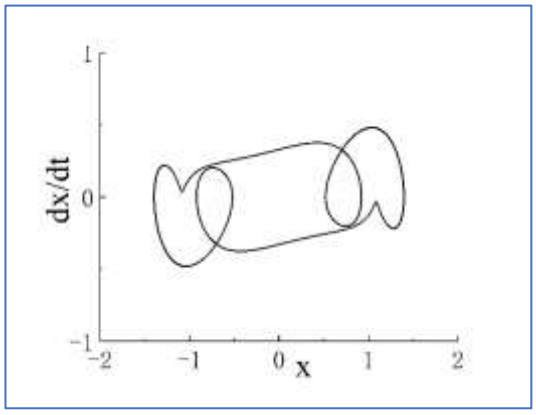

(c1)

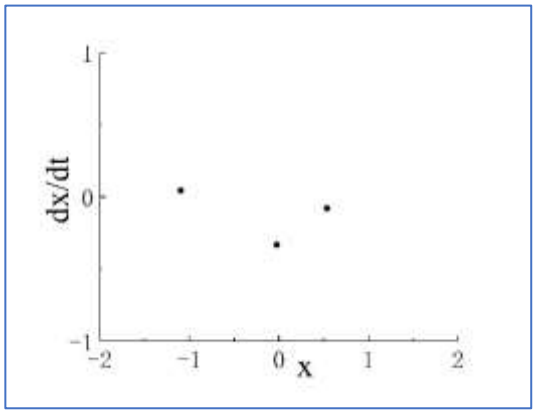

(c2)

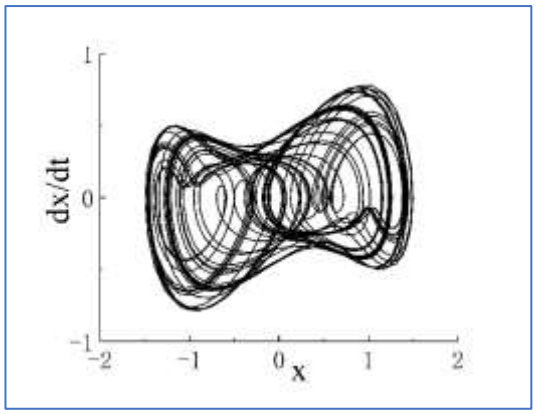

(d1)

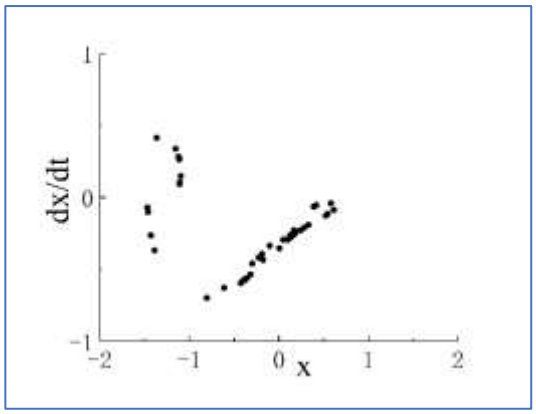

(d2)

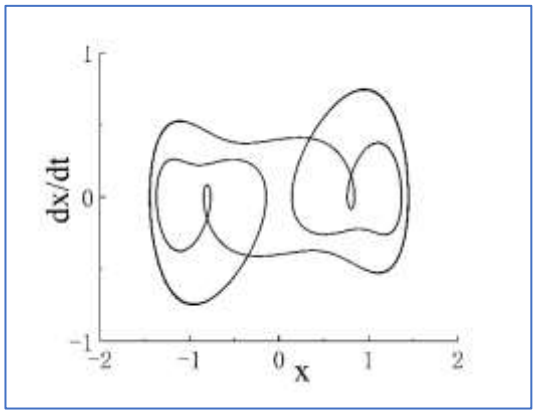

(e1)

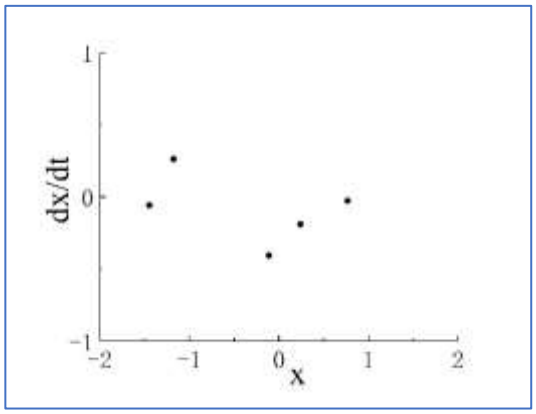

(e2)

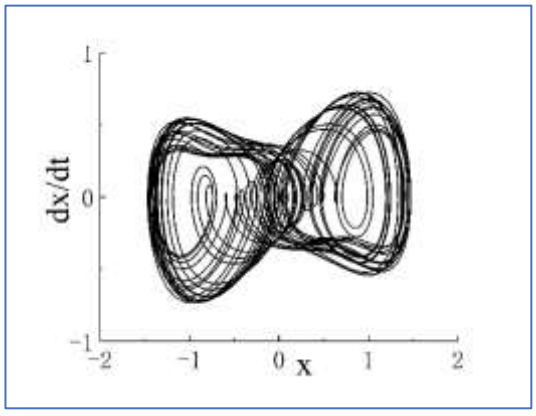

(f1)

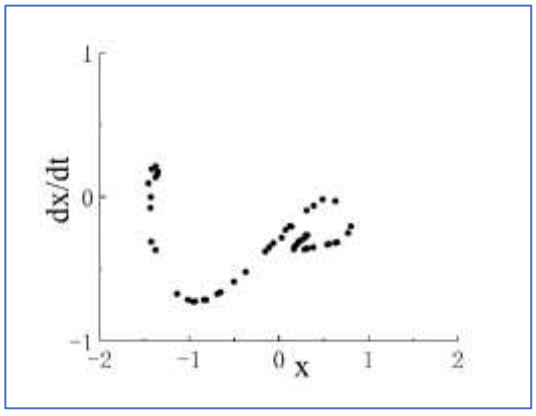

(f2)

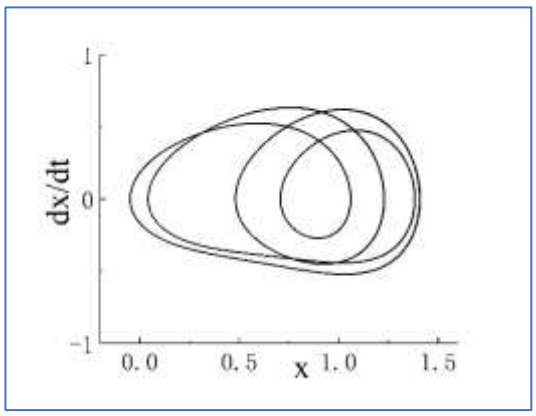

(g1)

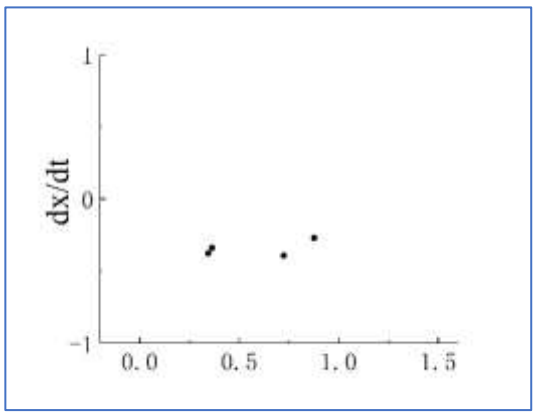

(g2)

Fig.2 Phase portraits and Poincaré maps of the fractional Duffing system. (a1) Phase portrait with $\omega = 0.45$, (a2) Poincaré map with $\omega = 0.45$, (b1) phase portrait with $\omega = 0.509$, (b2) Poincaré map with $\omega = 0.509$, (c1) phase portrait with $\omega = 0.55$, (c2) Poincaré map with $\omega = 0.55$, (d1) phase portrait with $\omega = 0.6$, (d2) Poincaré map with $\omega = 0.6$, (e1) phase portrait with $\omega = 0.8$, (e2) Poincaré map with $\omega = 0.8$, (f1) phase portrait with $\omega = 0.88$, (f2) Poincaré map with $\omega = 0.88$, (g1) phase portrait with $\omega = 1.02$ and (g2) Poincaré map with $\omega = 1.02$

Notably, periodic motion windows are present in the three chaotic motion regions. The bifurcation diagram of the periodic motion window in the first chaotic motion region is shown in Fig. 3(a). The chaotic motion transitions from period-doubling motion to period-2 motion. The phase portrait and Poincaré map when $\omega = 0.506$ in the period window are shown in Figs. 3(b) and 3(c), respectively. The bifurcation diagram of the periodic motion window in the second chaotic motion region is shown in Fig. 4(a). In the period window, $\omega = 0.635$ is period-4 motion, and its phase portrait and Poincaré map are shown in Figs. 3(b) and 3(c), respectively. Fig. 5(a) presents the bifurcation diagram of the periodic window in the third chaotic region. Figs. 5(b) and 5(c) respectively show the phase portrait and corresponding Poincaré map when $\omega = 0.904$ in the window.

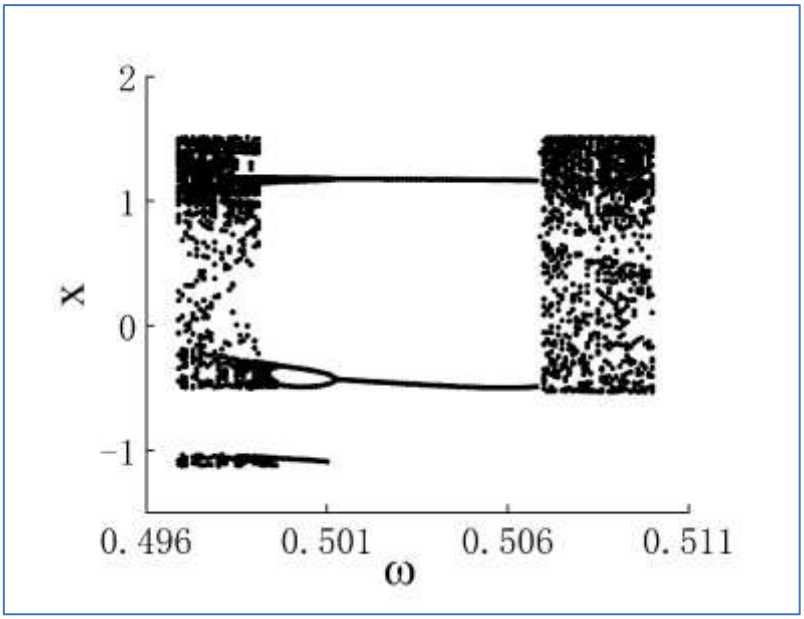

(a)

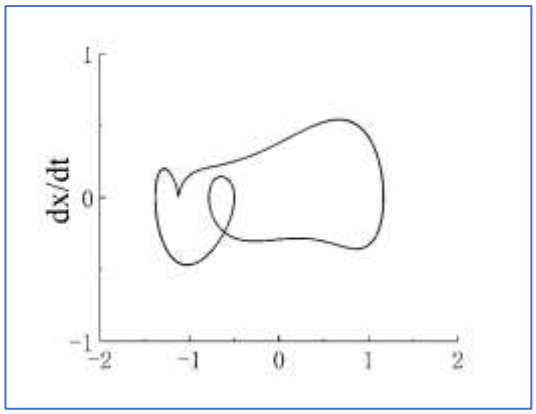

(b)

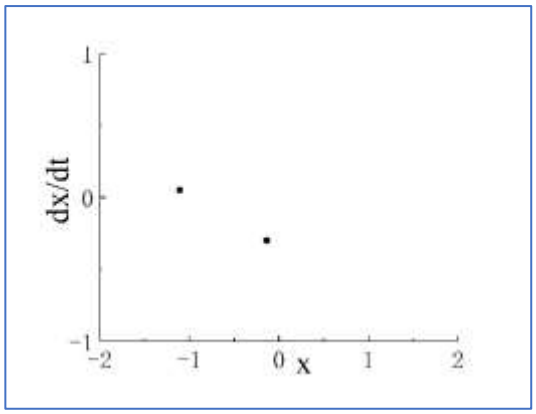

(c)

Fig.3 (a) Bifurcation diagram of the periodic window in chaotic motion region 1, (b) phase portrait when $\omega = 0.506$ and (c) Poincaré map when $\omega = 0.506$

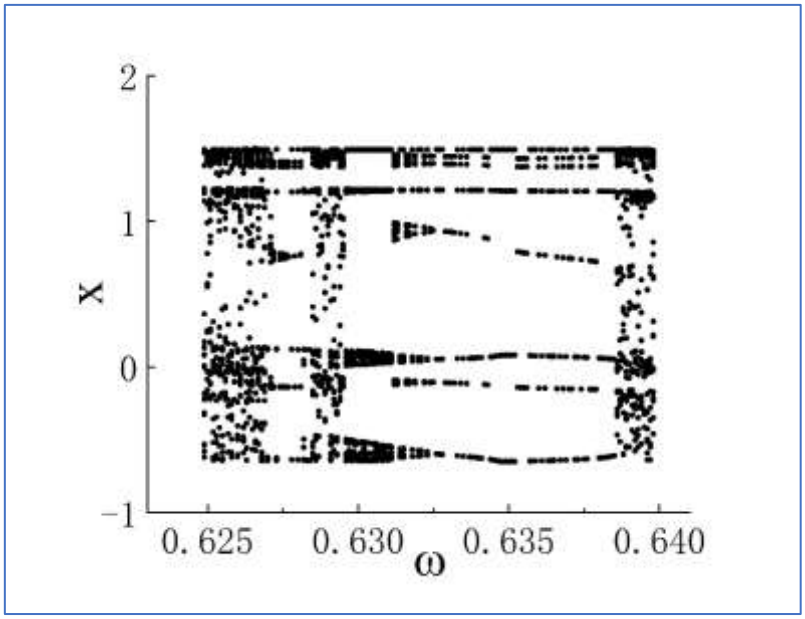

(a)

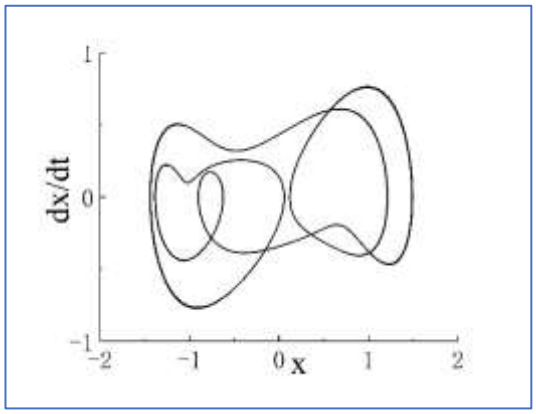

(b)

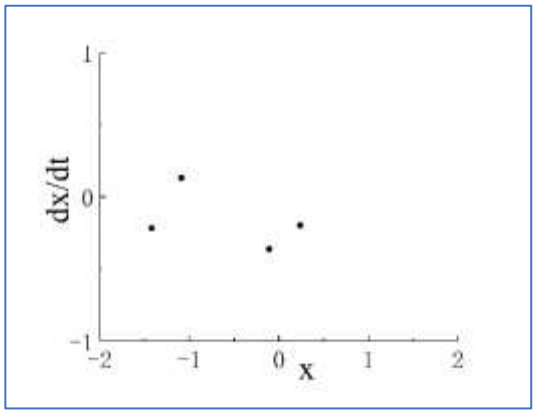

(c)

Fig.4 (a) Bifurcation diagram of the periodic window in chaotic motion region 2, (b) phase portrait when $\omega = 0.635$ and (c) Poincaré map when $\omega = 0.635$

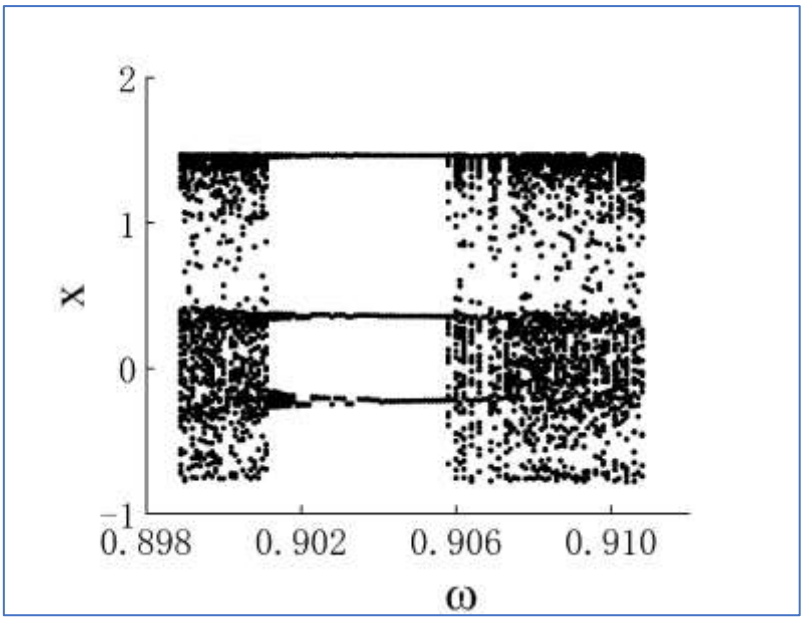

(a)

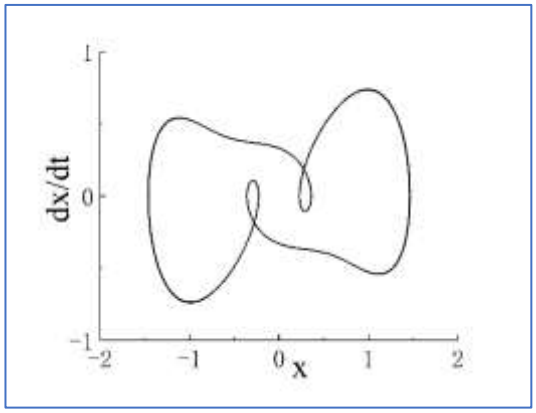

(b)

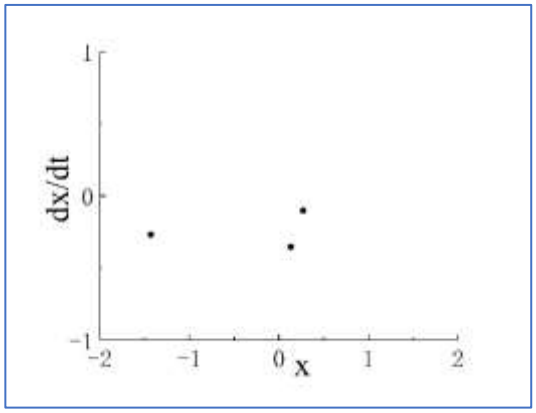

(c)

Fig.5 (a) Bifurcation diagram of the periodic window in chaotic motion region 3, (b) phase portrait when $\omega = 0.904$ and (c) Poincaré map when $\omega = 0.904$

Notably, an interesting change occurs in the periodic window of the second chaotic motion region. Although the system moves in period 4 in the window, the bifurcation diagram has eight dotted lines instead of four solid lines. Although the system exhibits period-4 motion in the period window, the bifurcation diagram has eight dotted lines instead of four solid lines. This observation shows that the motion of the system jumps with the change in frequency in the period window, but it is still period-4 motion. For example, the phase portraits when $\omega = 0.6352$ and $\omega = 0.6353$ are shown in Figs. 6(a) and 6(b), respectively. The phase portraits of two adjacent frequency points are rotated by exactly 180 degrees. When the frequency is further refined, this jumping

property remains. Figs. 6(c) and 6(d) present phase portraits with ω of 0.63280 and 0.63281, respectively.

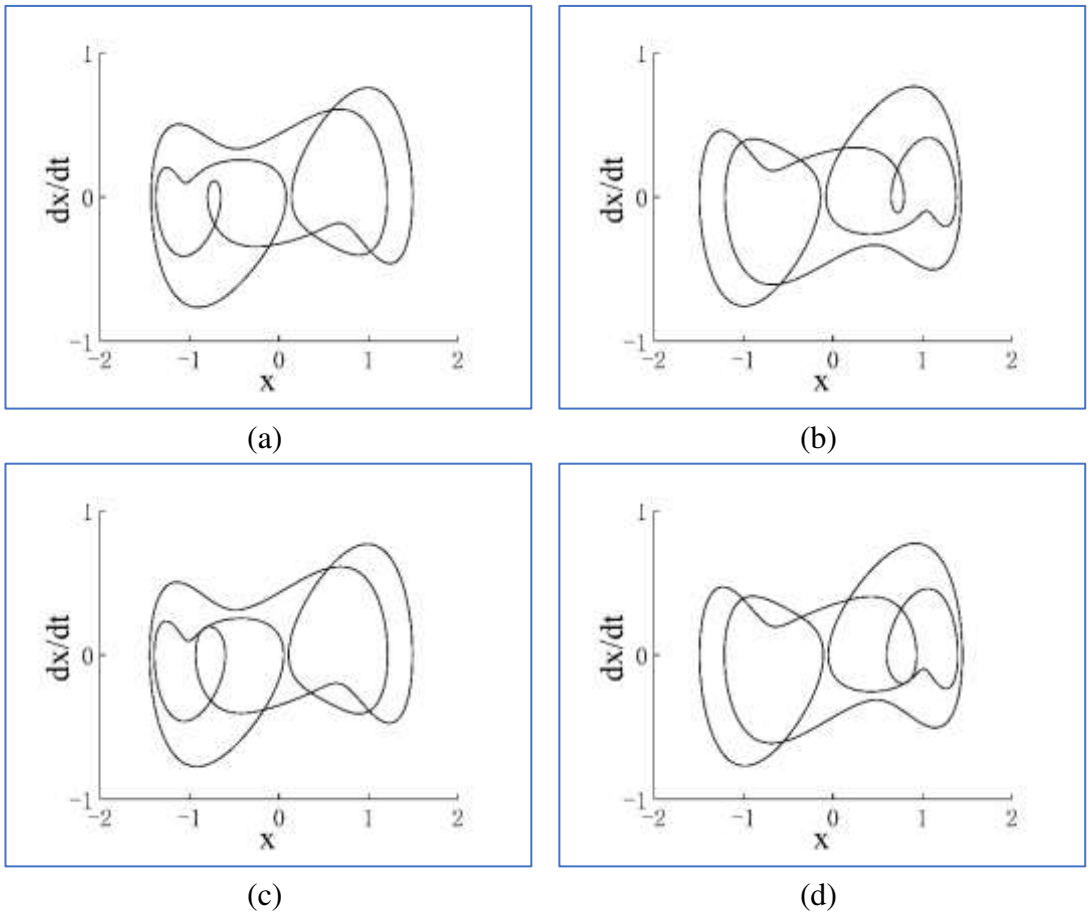

Fig.6 (a)Phase portrait with $\omega = 0.6352$, (b) phase portrait with $\omega = 0.6353$, (c) phase portrait with $\omega = 0.63280$ and (d) phase portrait with $\omega = 0.63281$

3.2 Fractional order α and excitation amplitude f are the change parameters

This work also examines the dynamic characteristics of the system when the fractional order changes. The excitation amplitude is $f = 1$, the excitation frequency is $\omega = 1$, the basic step length is $h = 0.001$, the basic truncation term is $Nt = 10{,}000$ and the step length magnification is $m = 5$. it's the memory weakens as the fractional order increases. Thus, the number of truncated items Nt is set to decrease by 1000 items with each increase in α by 0.2. The bifurcation diagram is shown in Fig. 7(a). In the process of changing fractional order α from 0.2 to 2, three periodic and three chaotic motion regions appear. The transition is from the first chaotic zone to a stable period-1 motion region after period-doubling bifurcation. As α continues to increase, it enters the second chaotic motion region through period-doubling bifurcation.

Fig. 7(b) presents the bifurcation diagram of the system when excitation amplitude f changes from 0.1 to 2.1. The fractional order is $\alpha = 0.8$, the excitation frequency is $\omega = 1$, the basic step length is $h = 0.001$, the basic truncation item number is $Nt = 10{,}000$ and the step length magnification is $m = 5$. The figure shows that three periodic and two chaotic motion regions appear during the change of excitation amplitude. The first is a stable period-1 motion; the first chaotic motion region is entered through period-doubling bifurcation, followed by entrance to the period-3 motion region. A part of the period-6 movement is contained in the period-3 motion region, and the second chaotic motion region is entered from period-3 motion. As the excitation amplitude continues to increase, the system transitions from the second chaotic region to the period-1 motion region through period-doubling bifurcation.

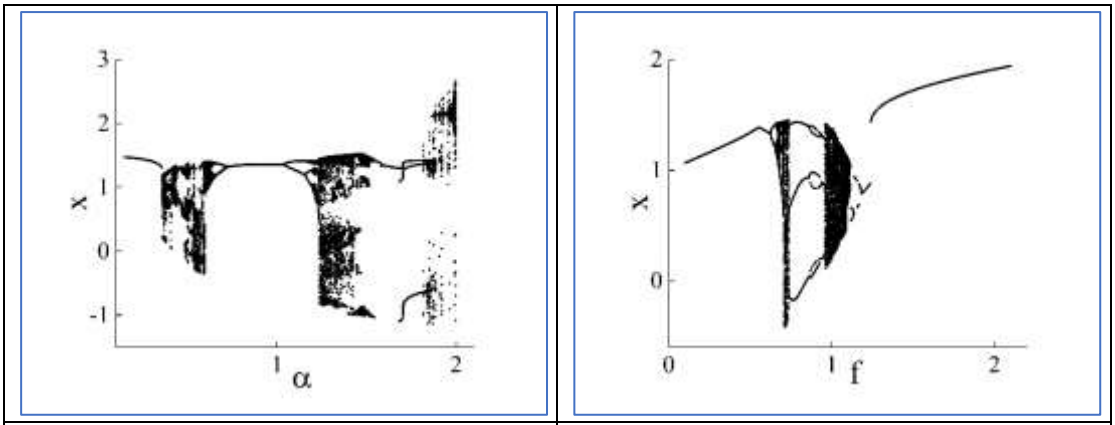

(a) (b)

Fig.7 (a)Bifurcation diagram of x versus α, $0.2 < \alpha < 2$ and (b) bifurcation diagram of x versus f, $0.1 < f < 2.1$

4. Conclusion

An improved short memory principle method is introduced to solve the fractional Duffing system numerically, and the basis for the improvement of the short memory principle method is provided. The influence of excitation frequency on the dynamic performance of the system is studied using nonlinear dynamic analysis methods, such as phase portrait, Poincaré map and bifurcation diagram. The bifurcation diagram has four periodic and three chaotic motion regions. The third chaotic motion region exhibits an obvious transition from period-doubling motion to stable period-1 motion. In addition, periodic motion windows are found in the three chaotic motion regions. The

periodic motion of the periodic window in the second chaotic motion region has a jumping property. The influence of excitation amplitude and fractional order on the dynamic performance of the system is also studied. The results show that a change in the system parameters of the fractional Duffing equation affects the dynamic performance of the system. Thus, such change should be given attention during dynamic system design and analysis.

Funding: This study was funded by the National Natural Science Foundation of China (Grant No.11472133).

Compliance with ethical standards.

Conflict of interest: The authors declare that they have no conflict of interest.

Dataset derived from public resources and made available with the article.

Reference

1. Oldham K B, Spanier J. The Fractional Calculus: Theory and Applications of Differentiation and Integration to Arbitrary Order. Dover Publications, Inc.
2. Cannon J W, Mandelbrot B B. The Fractal Geometry of Nature[J]. The American Mathematical Monthly, 1984.
3. Bagley R L, Torvik P J. Fractional calculus in the transient analysis of viscoelastically damped structures[J]. AIAA Journal, 1985, 23(6):918-925.
4. Bagley R L, Torvik P J. Fractional calculus - A different approach to the analysis of viscoelastically damped structures[J]. AIAA Journal, 2012, 21(5):741-748.
5. Yu Y, Li H X, Sha W, et al. Dynamic analysis of a fractional-order Lorenz chaotic system[J]. Chaos Solitons & Fractals, 2009, 42(2):1181-1189.
6. Hartley T T, Lorenzo C F. Chaos in a fractional order Chua's system[J]. IEEE Transactions on Circuits & Systems, 1995, 42(8):P.485-490.
7. Agrawal O P. A General Formulation and Solution Scheme for Fractional Optimal Control Problems[J]. Nonlinear Dynamics, 2004, 38(1-4):323-337.
8. Chen Y Q, Vinagre B M, Podlubny I. Continued Fraction Expansion Approaches to Discretizing Fractional Order Derivatives—an Expository Review[J]. Nonlinear Dynamics, 2004, 38(1-4):155-170.
9. Jimenez, S, Gonzalez, JA, Vazquez, L. Fractional Duffing's Equation and Geometrical Resonance[J]. International Journal of Bifurcation & Chaos, 2013, 23(05):1350089.
10. Jia J H, Shen X Y, Hua H X. Viscoelastic Behavior Analysis and Application of the Fractional Derivative Maxwell Model[J]. Journal of Vibration & Control, 2007, 13(4):385-401.
11. Shokooh, Arsalan, Suarez, et al. A Comparison of Numerical Methods Applied to a Fractional Model of Damping Materials.[J]. Journal of Vibration & Control, 1999, 5(3):331-354.

12. R. S. Barbosa, J. A. Tenreiro Machado. Describing Function Analysis of Systems with Impacts and Backlash [J]. Nonlinear Dynamics, 2002, 29(1/4):235-250.
13. Yu YG, Li HX, Wang S, Yu JZ. Dynamic analysis of a fractional-order Lorenz chaotic system. Chaos Solitons Fractals 2009;42:1181–9.
14. Hartley TT, Lorenzo CF, Qammer HK. Chaos in a fractional order Chua's system. IEEE Trans Circuits Syst 1995;42:485–90.
15. Zhang WW, Zhou SB, Li H, Zhu H. Chaos in a fractional-order Rossler ¨ system. Chaos Solitons Fractals 2009;42:1684–91.
16. Machado JAT, Baleanu D, Chen W, Sabatier J. New trends in fractional dynamics. J Vib Control 2014;20:963.
17. Li X, Wu RC. Hopf bifurcation analysis of a new commensurate fractional-order hyperchaotic system. Nonlinear Dyn 2014;78:279–88.
18. Chen DY, Wu C, Herbert HCI, Ma XY. Circuit simulation for synchronization of a fractional-order and integer-order chaotic system. Nonlinear Dyn 2013;73:1671–86.
19. Shen YJ, Wei P, Yang SP. Primary resonance of fractional-order van der Pol oscillator. Nonlinear Dyn 2014;77:1629–42.
20. Srinil N, Zanganeh H. Modelling of coupled cross-flow/in-line vortexinduced vibrations using double Duffing and van der Pol oscillators. Ocean Eng 2012;53:83–97.
21. Jimenez S, Gonzalez JA, Vazquez L. Fractional Duffing's equation and geometrical resonance. Int J Bifurc Chaos 2013;23:1350089.
22. Brzeski P, Perlikowski P, Kapitaniak T. Numerical optimization of tuned mass absorbers attached to strongly nonlinear Duffing oscillator. Commun Nonlinear Sci Numer Simul 2014;19:298–310.
23. Maia N, Silva J, Ribeiro A. ON A GENERAL MODEL FOR DAMPING[J]. Journal of Sound & Vibration, 1998, 218(5):749-767.
24. Hartley T T, Lorenzo C F. A Frequency-Domain Approach to Optimal Fractional-Order Damping[J]. Nonlinear Dynamics, 2004, 38(1-4):69-84.
25. Yan W, An J Y. Amplitude–frequency relationship to a fractional Duffing oscillator arising in microphysics and tsunami motion[J]. Journal of Low Frequency Noise Vibration and Active Control, 2018,38(3-4):1008-1012.
26. Li Z, Chen D, Zhu J, et al. Nonlinear dynamics of fractional order Duffing system[J]. Chaos Solitons & Fractals the Interdisciplinary Journal of Nonlinear Science & Nonequilibrium & Complex Phenomena, 2015, 81:111-116.
27. Duan J S, Sun J, Chao-Lu T. Nonlinear Fractional Differential Equation Combining Duffing Equation and Van Der Pol Equation[J]. Journal of Mathematics, 2011.
28. Niu J, Liu R, Shen Y, et al. Chaos detection of Duffing system with fractional-order derivative by Melnikov method[J]. Chaos, 2019, 29(12):123106.

Figures

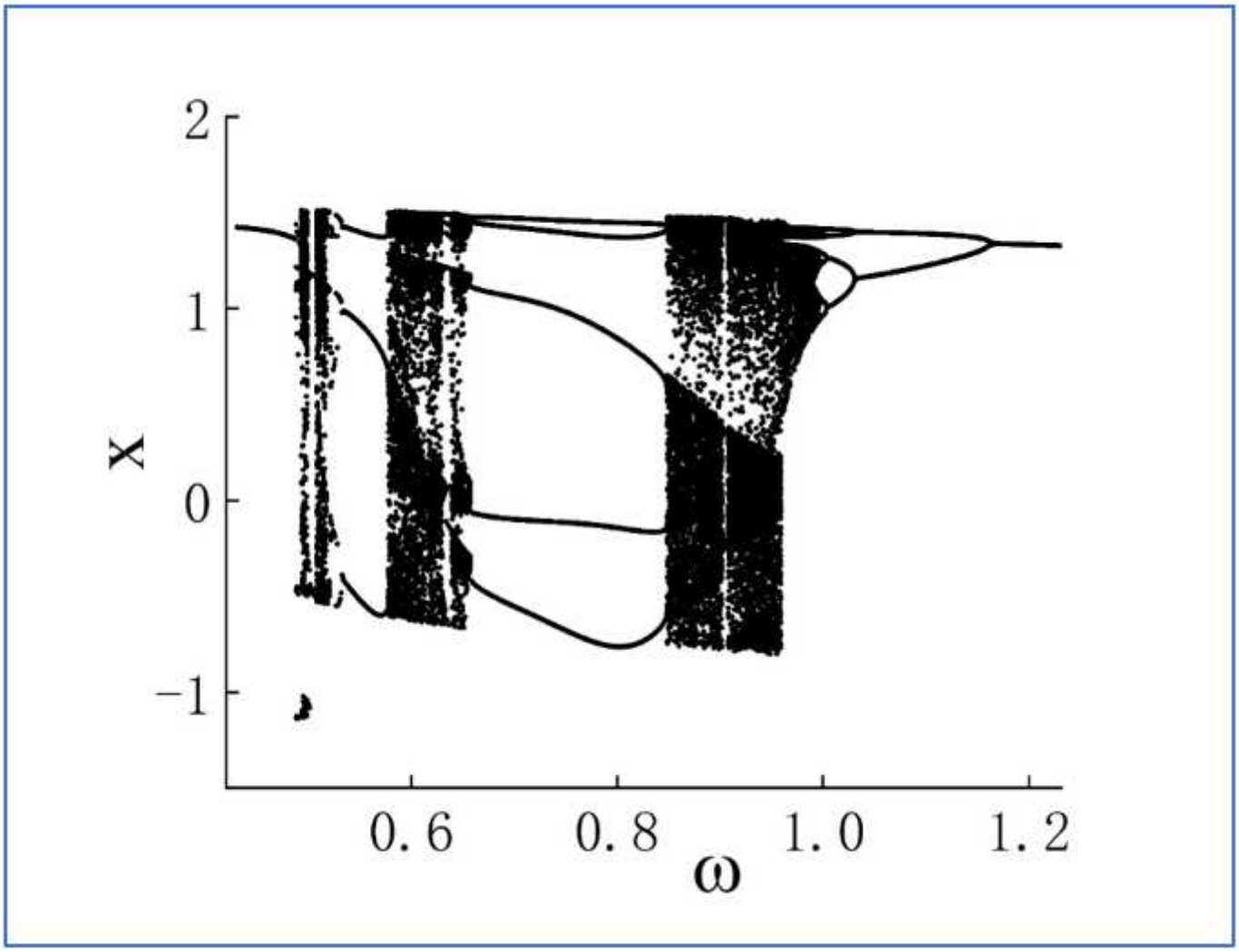

Figure 1

Bifurcation diagram of the fractional-order Duffing system with α=1.2, 0.43<ω≤1.23

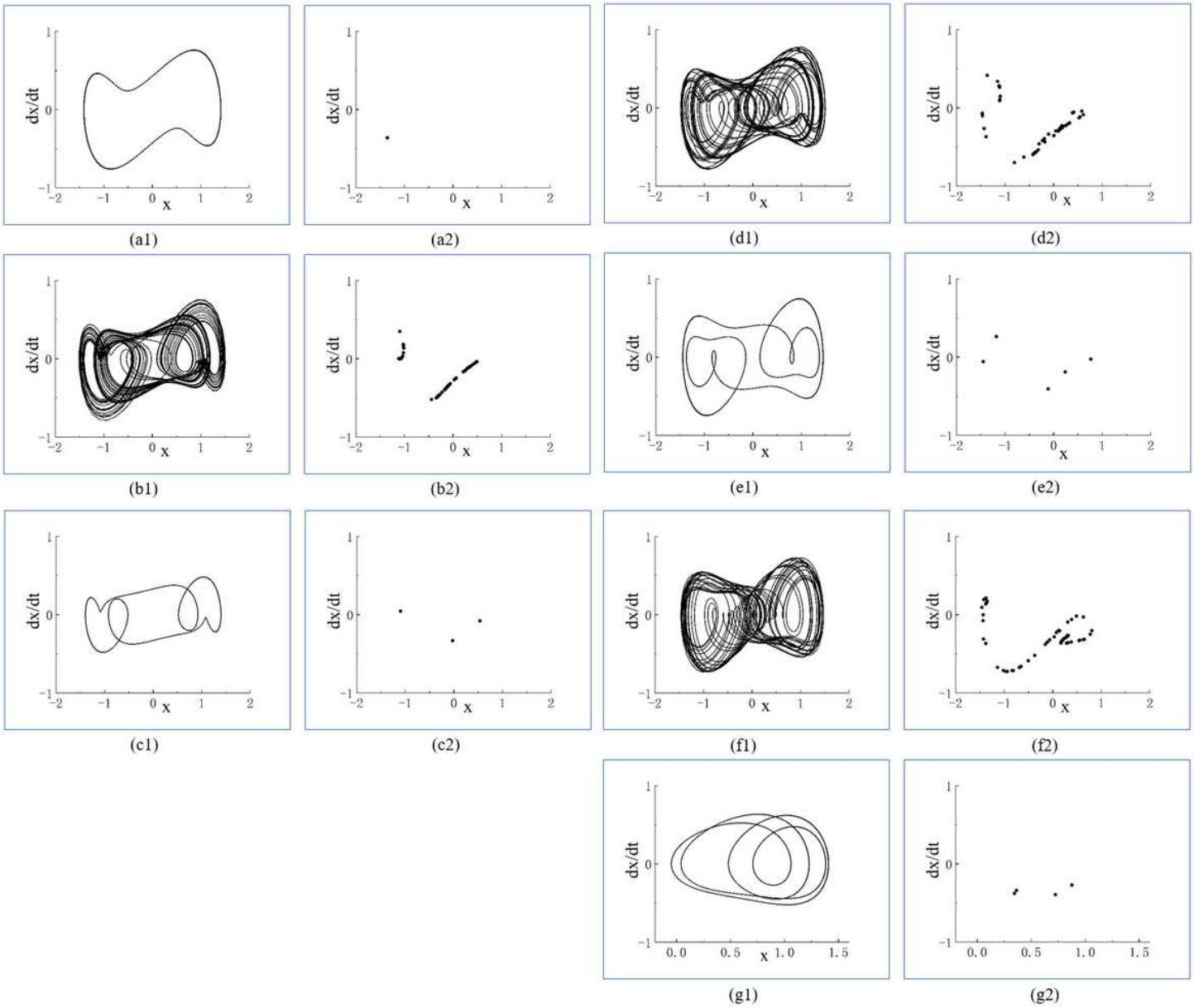

Figure 2

Phase portraits and Poincaré maps of the fractional Duffing system. (a1) Phase portrait with ω=0.45, (a2) Poincaré map with ω=0.45, (b1) phase portrait with ω=0.509, (b2) Poincaré map with ω=0.509, (c1) phase portrait with ω=0.55, (c2) Poincaré map with ω=0.55, (d1) phase portrait with ω=0.6, (d2) Poincaré map with ω=0.6, (e1) phase portrait with ω=0.8, (e2) Poincaré map with ω=0.8, (f1) phase portrait with ω=0.88, (f2) Poincaré map with ω=0.88, (g1) phase portrait with ω=1.02 and (g2) Poincaré map with ω=1.02

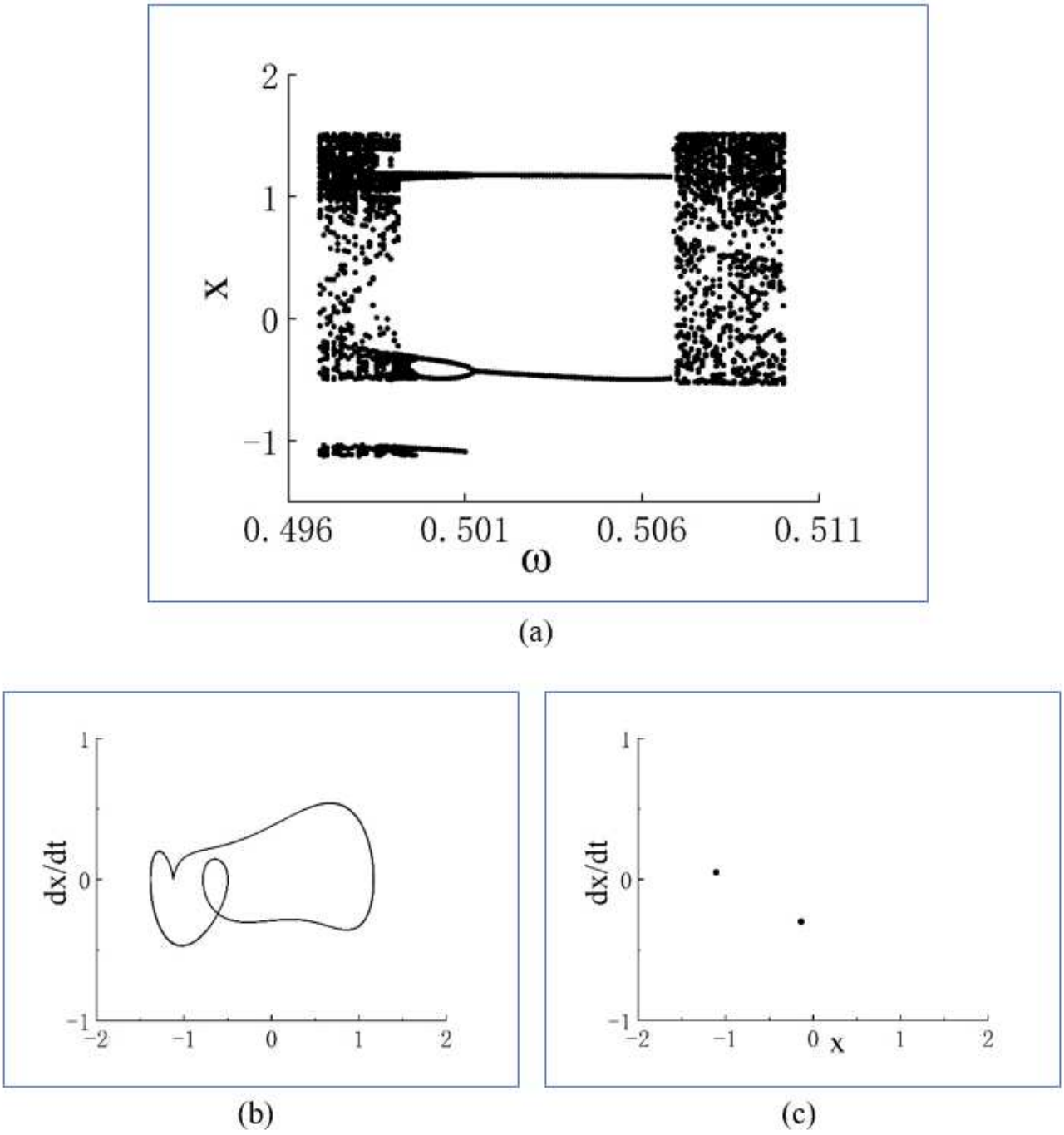

Figure 3

(a) Bifurcation diagram of the periodic window in chaotic motion region 1, (b) phase portrait when ω=0.506 and (c) Poincaré map when ω=0.506

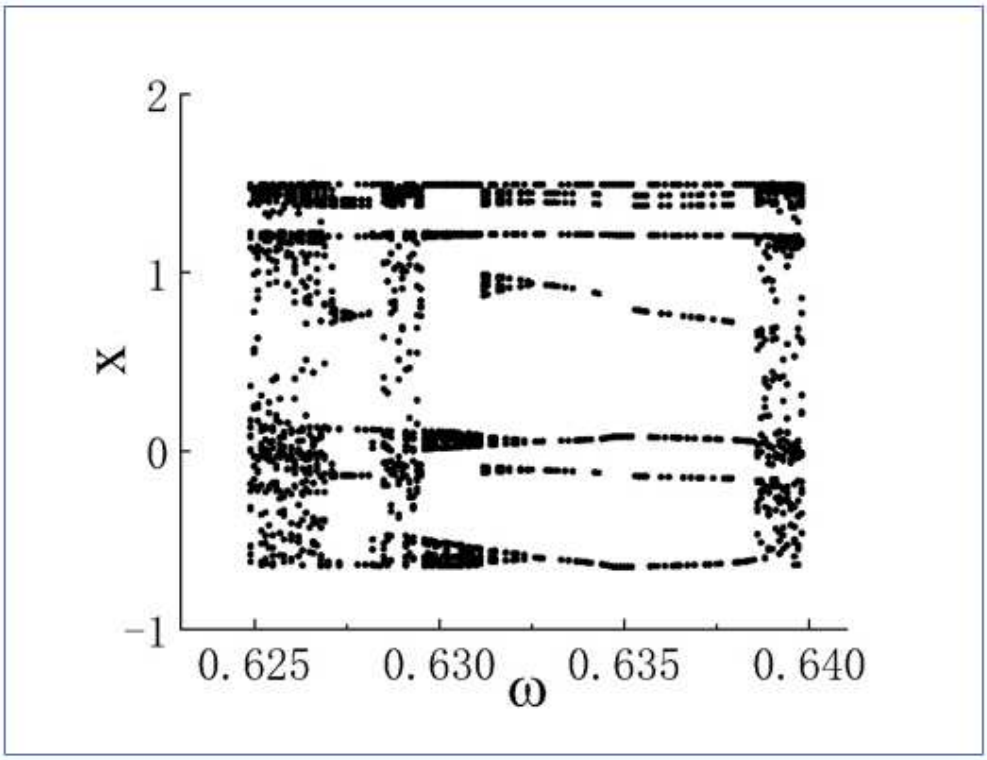

(a)

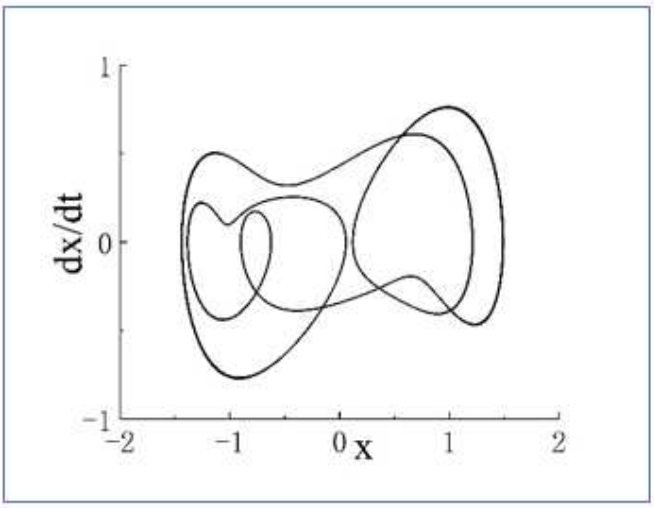

(b)

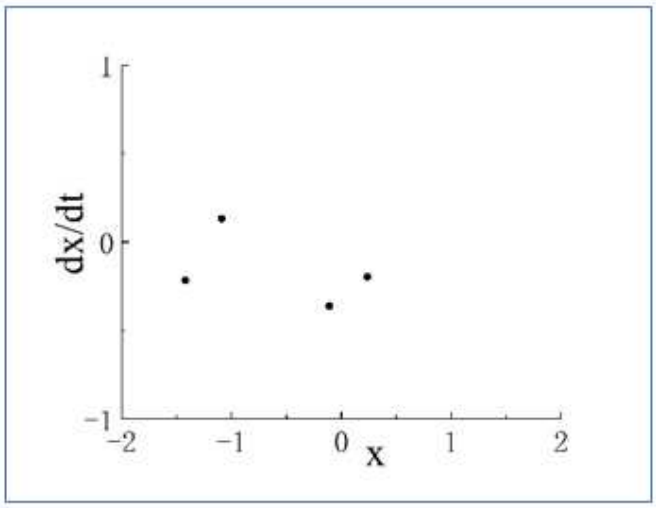

(c)

Figure 4

(a) Bifurcation diagram of the periodic window in chaotic motion region 2, (b) phase portrait when ω=0.635 and (c) Poincaré map when ω=0.635

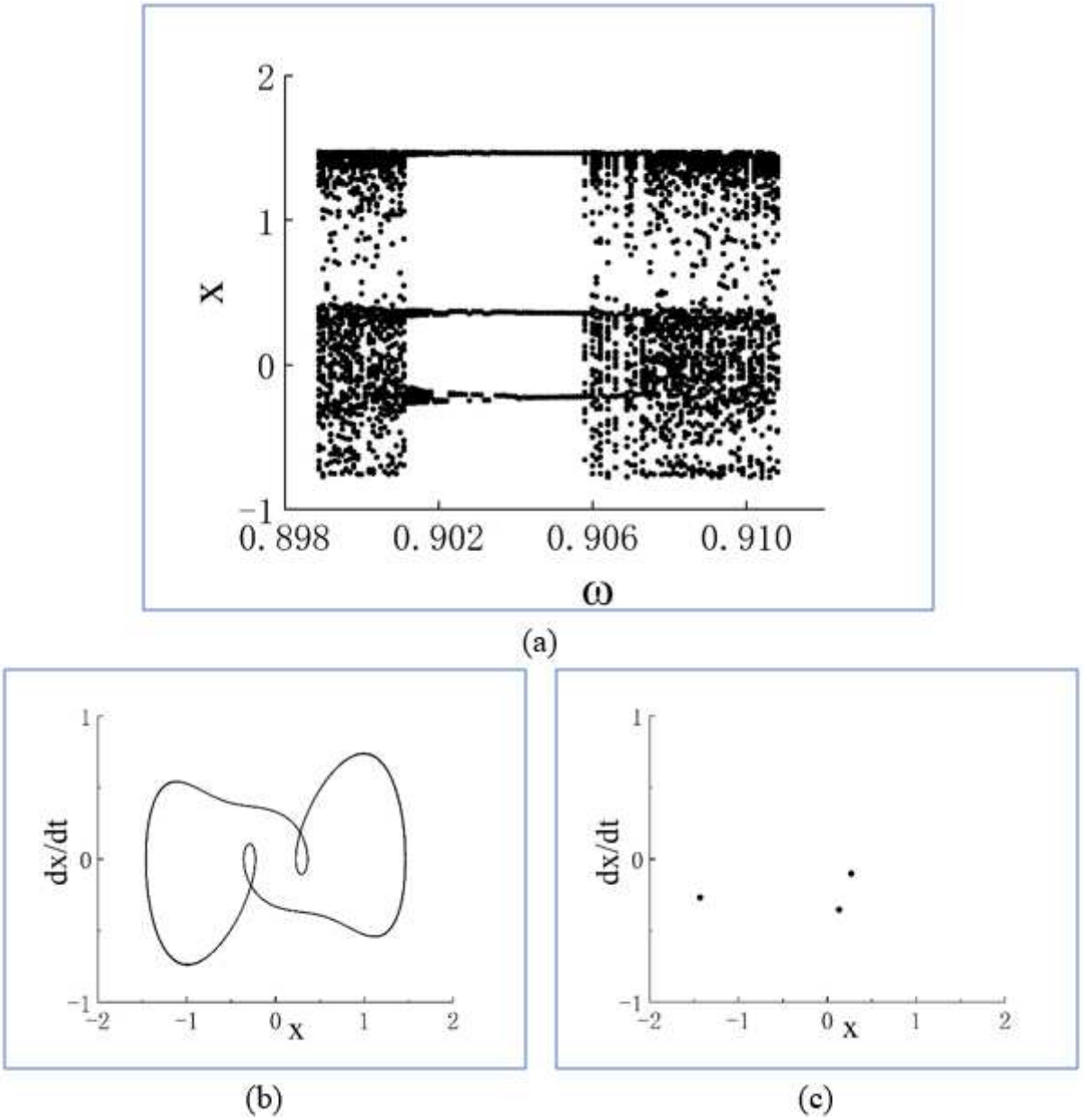

Figure 5

(a) Bifurcation diagram of the periodic window in chaotic motion region 3, (b) phase portrait when ω=0.904 and (c) Poincaré map when ω=0.904 Notably, an interesting change occurs in the periodic window of the second chaotic

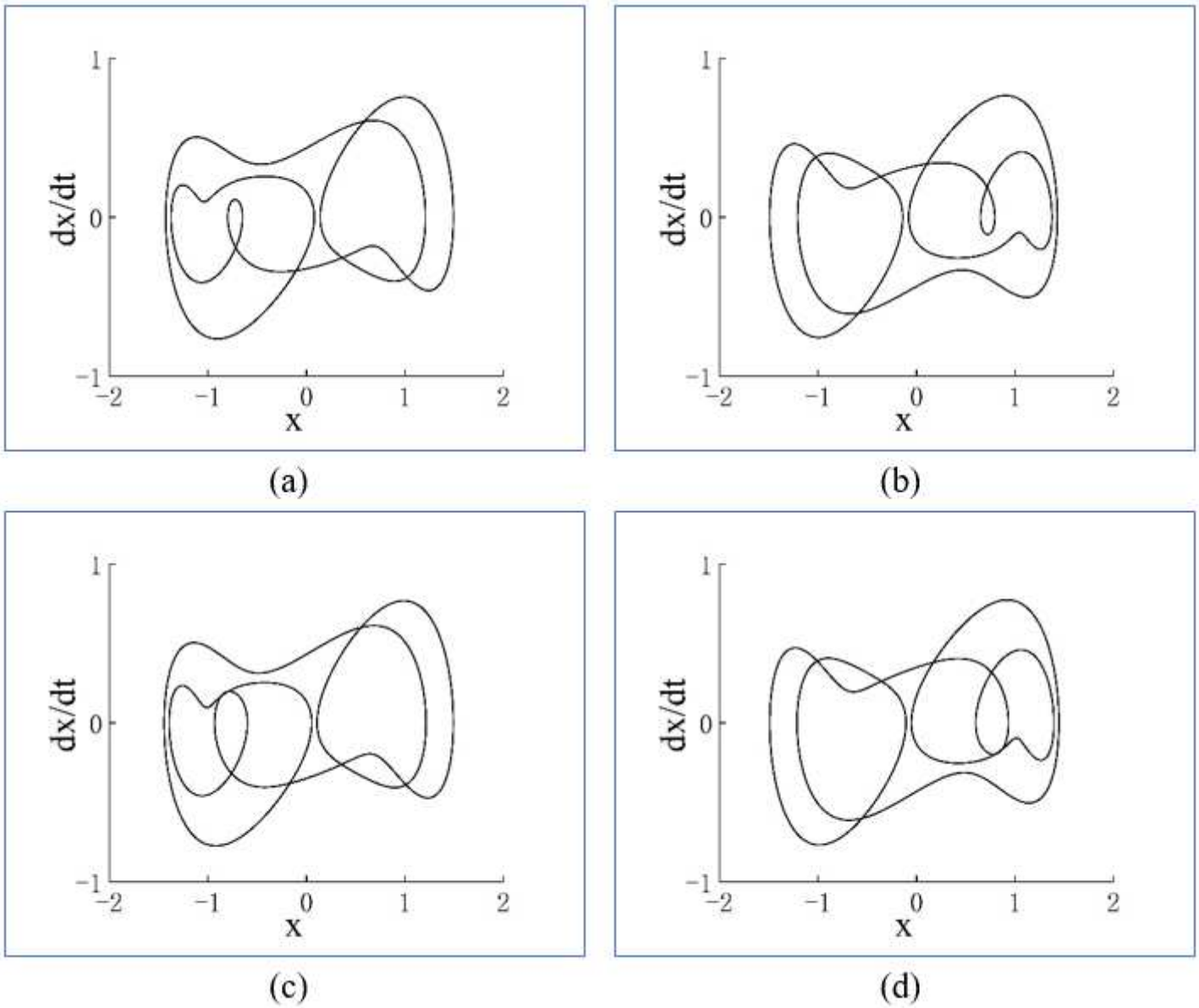

Figure 6

(a)Phase portrait with ω=0.6352, (b) phase portrait with ω=0.6353, (c) phase portrait with ω=0.63280 and (d) phase portrait with ω=0.63281

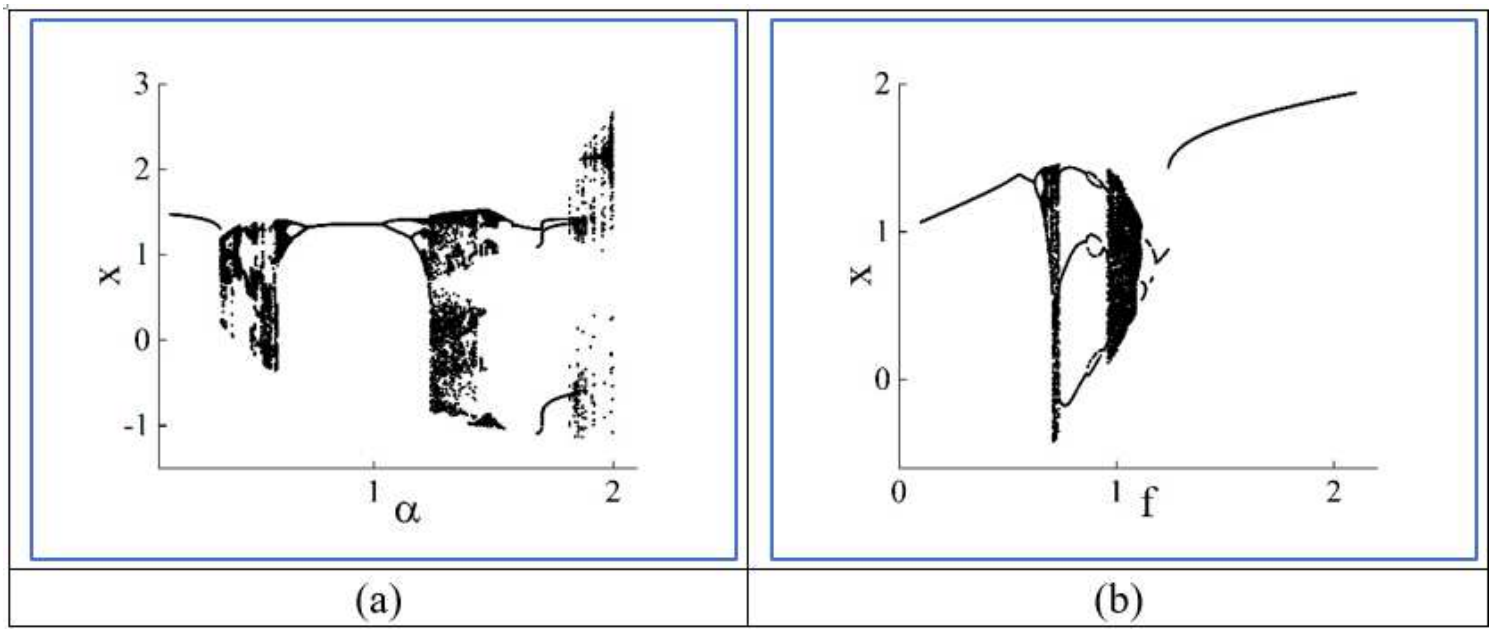

Figure 7

(a)Bifurcation diagram of x versus α, 0.2<α<2 and (b) bifurcation diagram of x versus f, 0.1